DESY 95-207

TESTS OF QCD WITH HADRONIC FINAL STATES IN DEEP INELASTIC SCATTERING

Ulrich Goerlach*
Deutsches Elektronen Synchrotron
Notkestraße 85, D-22607 Hamburg

Invited talk given at the
XV International Conference on Physics in Collisions
Cracow, Poland, June 8–10, 1995.

Abstract

New results on hadronic final states in deep inelastic scattering from the two experiments H1 and ZEUS at HERA are presented. The analysis of the hadronic system addresses the physics of multi-jet events, the validity of the DGLAP and BFKL evolution equations and the transition regime between soft and hard pomeron exchange.

In the region at low $x_{Bj} \approx 10^{-3}$ where the structure function F_2 is strongly rising the average E_T flow is at a level of 2 GeV per unit of rapidity. This E_T flow and the forward jet production rate are consistent with theoretical calculations based on the BFKL dynamics.

The observation of multiple jets permits the direct measurement of the gluon density in the proton at low x_{Bj}. The running coupling constant α_s is determined as a function of Q in a single experiment. The extrapolation to the Z^0-mass gives $\alpha_s(M_Z) = 0.123 \pm 0.012 \pm 0.013$ and $\alpha_s(M_Z) = 0.117 \pm 0.005^{+0.008}_{-0.009}$ for H1 and ZEUS, respectively.

The measurement of the cross section for ρ^0 and J/ψ vector meson production at low and high Q^2 shows an onset of hard perturbative QCD processes whenever the involved scale, the mass or Q, is larger than 2–3 GeV. This onset is visible in a steep rise of the cross section as a function of the γ^*-proton center of mass energy. It can be interpreted as a consequence of the rising gluon density of the proton. This behaviour of the cross section indicates a transition between a regime of soft and hard pomeron exchange.

*presenting results of the H1 and ZEUS collaborations

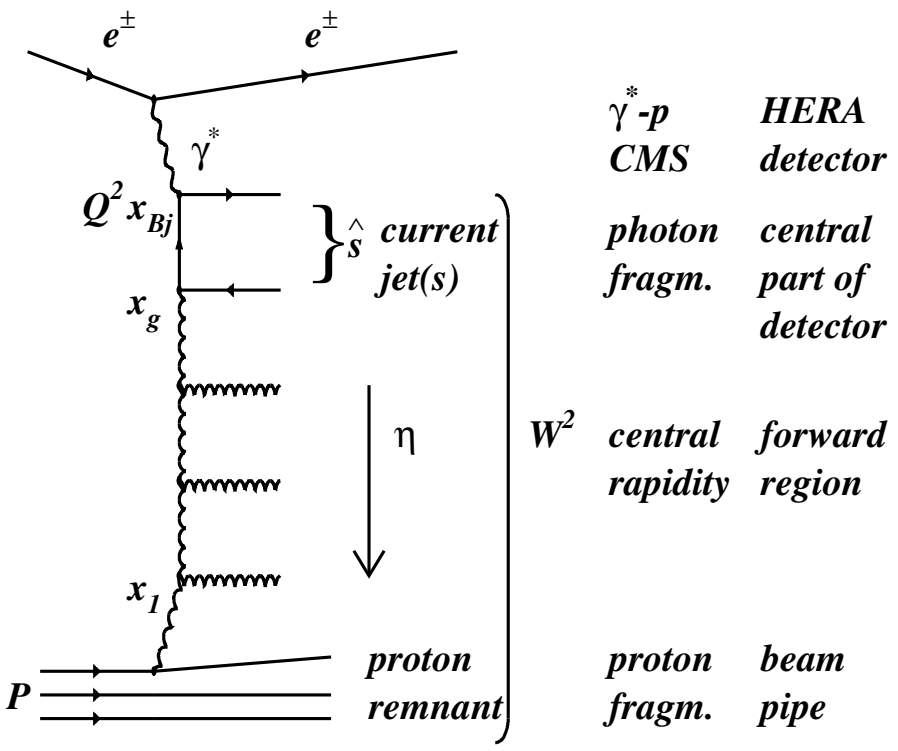

Figure 1: Graph of deep inelastic lepton scattering including hadronic final state production. The right hand side indicates the rapidity space in the $\gamma^* p$ center of mass system(CMS) and the corresponding regions of the HERA detectors.

1 Introduction

Deep inelastic lepton scattering (DIS) has provided much of the experimental insight into the structure of hadronic matter. The scaling behaviour of structure functions led to the quark parton model of the proton. The subsequent observation of scaling violations and their understanding in the framework of Quantum-Chromo-Dynamics (QCD) has not only revealed the gluon content of the proton but also helped to establish QCD as the theory of strong interactions.

1.1 DIS at HERA

With the start-up of HERA at DESY, where a 820 GeV proton beam collides with an electron or positron beam of 27 GeV, the field of deep inelastic lepton scattering has received a considerable boost, both from experiment and from theory. This is because of the enlarged kinematic region accessible to the experiments. With the high $\sqrt{s}$ of about 300 GeV large values of Q^2 up to 10^4 GeV^2 and Bjørken x as low as 10^{-5} at $Q^2 = 1$–5 GeV^2 can be reached.

A simplified graph for the scattering process is shown in Fig. 1. The lepton interacts only with the quarks of the proton via the exchange of a virtual photon or, at very high energies, a virtual Z^0 or W boson. The quark might be a valence quark, or a sea quark generated by the gluon field in the proton. This is the case especially at low x_{Bj} . The upper part of Fig. 1

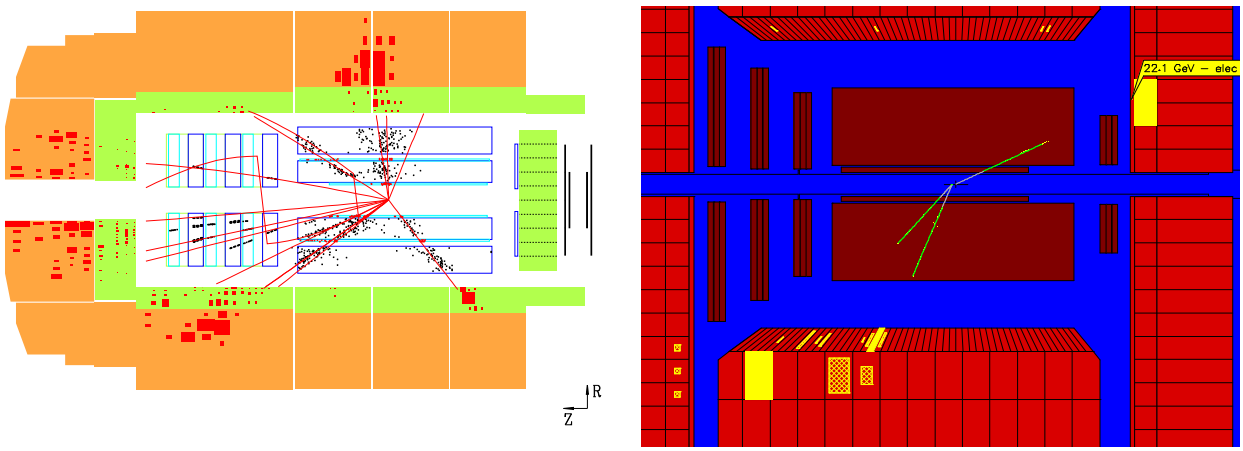

Figure 2: Left: (2+1) jet event in the H1 detector at HERA. The proton beam comes from the right hand side, the electrons from the left.

Figure 3: Right: An elastic ρ^0-DIS event in the very central part of the ZEUS detector. The scattered electron is seen in the rear calorimeter on the right.

shows the scattering off a struck sea quark in the proton, whereas the lower part illustrates the evolution of the gluons through several gluon splitting vertices.

The kinematics of deep inelastic scattering can be described by two independent variables related to the lepton scattering angle and the energy loss of the lepton. In DIS the quantities chosen for the analysis are the square of the four momentum transfer $Q^2 = -q^2 = -(p_e - p_{e'})^2$ and the fractional energy transfer of the electron to the proton in the proton rest frame $y = q \cdot p / p_e \cdot p$; p and p_e are the four momentum vectors of the proton and the lepton, respectively. They are related to the Bjørken scaling variable $x_{Bj} = Q^2/2p \cdot q$ and the center of mass energy $\sqrt{s}$ via the relation $Q^2 = x_{Bj} \cdot y \cdot s$.

In the case of very small $Q^2 \ll 1$ GeV^2 the photon is quasi-real and these collisions are often referred to as photo production. For these events the electron is deflected by only a very small angle and escapes normally through the beam pipe. Experimentally at HERA all events with the electron detected in the central part of the detectors are called DIS. They cover roughly the regime of $Q^2 \gtrsim 5$ GeV^2. Events for which the electron is detected in the luminosity calorimeters at very small angles or escapes undetected are called tagged or untagged photo production events, respectively.

A detailed description of the two large HERA detectors H1[1] and ZEUS[2] can be found elsewhere. Fig. 2 and 3 show the central part of the two detectors comprising sophisticated tracking detectors in a magnetic field surrounded by high performance calorimeters. Not visible are the muon systems based on magnetized iron.

The results found in the regime of low x_{Bj} are striking: The structure function $F_2(x, Q^2)$ is rising at very low x [3, 4]. Also the gluon density grows rapidly. This rise is related to the nature of the QCD-evolution of the parton densities. However, at present on the basis of the structure function data alone it is not possible to distinguish between different evolution schemes. This is discussed by J. Ciborowsky in the previous contribution to these proceedings [5].

1.2 Hadronic Final States in DIS

Traditionally only the scattered electron was measured to determine the kinematic variables x_{Bj} and Q^2. In the case of lepton scattering at the HERA collider the final state formed by the hadronization of the struck quark can be observed within the detector much more clearly than in fixed target experiments. It is used as an additional method to determine the kinematics of the event. The study of the hadronic final state also provides other useful information about the underlying physics.

In Fig. 2 the clear jet structure of these events can be seen in the display of a high Q^2 event in the H1 detector. Two jets are observed in the central part of the detector. At HERA these jets are called current jets. An additional jet from the fragmentation of the proton remnant is partially seen very close to the beam pipe, the remnant jet. The convention is to count only the current jets and to add a (+1) to account for the remnant jet, irrespective of its visibility in the detector. The event of Fig. 2 is called a (2+1) jet event. The hadronic system is characterized by its total mass $W^2 = (q+p)^2 = y \cdot s \cdot (1 - x_{Bj}) + m_p^2$. The invariant mass of the subsystem, in this case the 2-jet system is called $\sqrt{\hat{s}}$. Several topics can be addressed in the study of such hadronic final states.

- *Jet properties:* the study of current jet fragmentation is similar to the analysis of jets in (e^+e^-) or proton colliders. Except for some subtle effects jet universality is found in these analyses [6] and will not be the subject of this paper.
- *Multi-jet systems:* the measurement of cross sections, jet asymmetries and relative rates of (2+1) and (1+1) jet events allows the determination of the strong coupling constant α_s as a function of Q^2 and a direct determination of the gluon distribution in the proton.
- *E_T flow and jet production close to the forward region:* the question of the nature of the QCD evolution at low x_{Bj} has become one of the most interesting question to be addressed at HERA. As it will be discussed below, E_T flow and jet production rates might be sensitive to the nature of the evolution.
- *Vector meson production:* final states like elastically produced ρ^0-mesons are of interest for the understanding of the nature of the pomeron. An example is shown together with the scattered electron in Fig. 3 of the ZEUS detector Such events can also be used to measure the gluon density in the proton.
- *Rapidity gap events:* these are a special group of events with no energy flow in the rapidity region close to the remnant are of Diffractive nature and are treated in the contribution by A. Brandt[7]

In the following section possible signatures are discussed to investigate the QCD evolution of parton densities. The section thereafter deals with the analysis of multi jet events for the determination of α_s and the gluon density in the proton. In the last part of the paper the production of vector mesons is investigated.

The data presented in this review were collected during the years 1993 and 1994 by the two experiments H1 and ZEUS with electron-proton and positron-proton collisions, respectively.

2 QCD Evolution at Low x

The strong rise of the F_2-structure function at low x has caused much debate on whether the HERA data are still in a regime where the QCD evolution can be described by the DGLAP (Dokshitzer-Gribov-Lipatov-Altarelli-Parisi)[8] evolution equations, or whether they

extend into a new regime where the dynamics is described by the BFKL (Balitsky-Fadin-Kuraev-Lipatov) equation[9]. To discuss the differences between the two, we look at Fig. 1 in more detail. The hadronization of the radiated gluons (and $q\bar{q}$-pairs) generated by the evolution from the proton to the $\gamma^* - q$ scattering vertex leads to a flow of particles which spans the rapidity interval between the forward going proton remnant and the fragmentation of the virtual photon. The current hemisphere containing the photon-fragmentation covers roughly the barrel parts of the HERA detectors.

The transverse energy, E_T, the number of jets etc. which can experimentally be observed between the proton and photon fragmentation region is sensitive to the details of the evolution which gives energy and transverse momentum to the partons. In lowest order the DGLAP and BFKL evolution equations effectively resum leading logarithmic contributions of type $\alpha_s \cdot \ln Q^2$ and $\alpha_s \cdot \ln(1/x)$, respectively. In the leading log DGLAP scheme, applicable at not too small x_{Bj} ($\gtrsim 10^{-2}$), the parton cascade resulting from the evolution follows a strong ordering in transverse momentum $k_{T1} \ll ... \ll k_{Tn} \ll Q^2$, but only a weak ordering in Bjørken x, $x_1 \geq ... \geq x_n \geq x_{Bj}$. On the contrary, the BFKL scheme, supposedly valid in the very low $x_{Bj}(\lesssim 10^{-3})$ region, leads to strong ordering in x: $x_1 \gg ... \gg x_n = x_{Bj}$ but no ordering in k_T [10]. The energy flow and the production rate of jets between the photon and proton fragmentation region can be examined for differences between the two schemes. Two results are presented in the following.

2.1 Transverse Energy Flow

The E_T-flow at the parton level has been calculated as a function of rapidity by Kwiecinski et al.[11, 12, 13]. The authors come to the striking conclusion that in the case of a BFKL evolution the E_T-flow at central rapidity in the $\gamma^* p$ center of mass system (CMS) should be enhanced by 1.5–2 GeV relative to the expectation of the DGLAP evolution scheme. Further, the E_T-flow is predicted to increase with decreasing x_{Bj}.

The comparison with experiment is not straight forward: first of all it has to be noted that the central rapidity region in the hadronic CMS corresponds to the forward region $2 \lesssim \eta_{lab} \lesssim 4$ of the detectors. This area is affected by energy leakage through the beam hole in the calorimeters. Also possible contributions from overlap by the remnant fragmentation have to be accounted for.

Secondly, the measured energy in the detectors has to be corrected to the parton level in order to compare with the prediction (or vice versa). Two available Monte Carlo programs are used by the H1 and ZEUS experiments: the MEPS (Matrix Elements plus Parton Showers) and CDM (Colour Dipole Model, with the matrix element for the boson gluon fusion (BGF) process added). The MEPS is an option of the LEPTO generator [14] based on the DGLAP dynamics. Consequently, the emitted partons are strongly ordered in k_T. Such an ordering is not present in CDM[15] in which emitted gluons form independently radiating dipoles[16, 17]. However, the BFKL equations are not explicitly used.

In Fig. 4 the flow of transverse energy as measured in the ZEUS experiment[18] (1994 preliminary data, $Q^2 \geq 6$ GeV^2 and $x_{Bj} \geq 2 \cdot 10^{-4}$) is plotted as a function of rapidity and compared to the two models discussed above. In general, we can observe, that the present version of the MEPS program underestimates the measured energy flow of about 2 GeV per unit of rapidity in the forward region, whereas CDM(BGF) approximately generates this level of E_T. Both models do not describe very well the E_T-flow in the current region, especially not at low x.

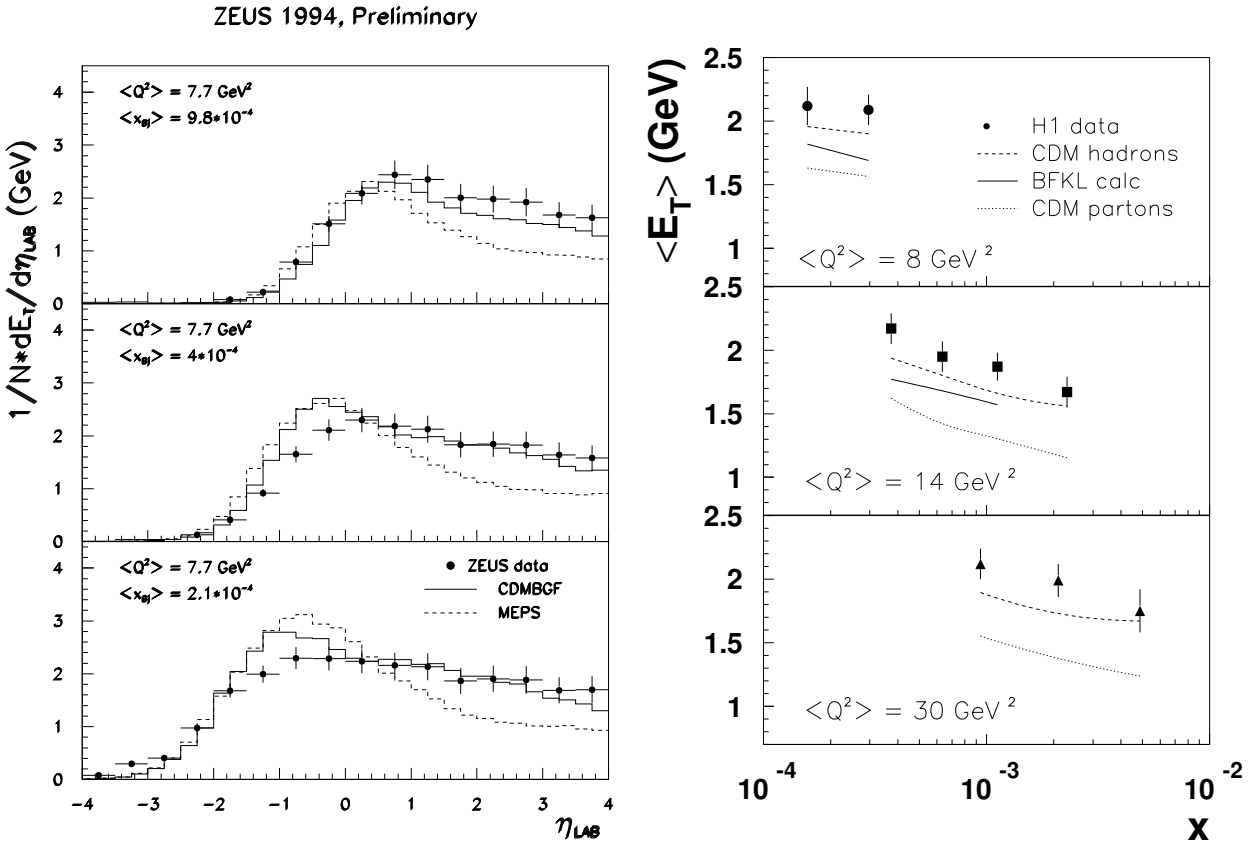

Figure 4: Transverse energy flow measured by the ZEUS detector as a function of pseudo-rapidity in the laboratory for different bins in x at fixed Q^2 and a comparison to the MEPS and the CDM(BGF) Monte Carlo.

Figure 5: Average transverse energy $< E_T >= 1/N \cdot dE_T/d\eta^*|_{\eta^*=0}$ at central pseudo-rapidity in the $\gamma^* - p$ CMS system as a function of Bjørken x for three different values of Q^2 (H1, 1993 data).

A slightly different way to look at the data is presented in Fig. 5 for the data of H1[19]: the E_T-flow at central rapidity in the hadronic CMS is shown as a function of x_{Bj} for three bins in Q^2 and $y > 0.05$. They observe a slight increase of E_T towards small x_{Bj} as predicted for BFKL. A direct comparison with calculations on the parton level[13] is not possible. However, in order to estimate the effect of hadronization the prediction of CDM is plotted at the parton level and after hadronization. This gives a contribution of roughly 500 MeV to the E_T-flow. Adding this level to the BFKL calculation would bring it very close to the data.

The failure of the MEPS program should not be over-interpreted. The missing amount of E_T is of similar order as the contribution from hadronization which is not yet optimized in this model for this type of studies. Work is underway to investigate this.

It is interesting to look at the data on energy flow in a slightly different way. From hadron collisions we know that particle production and energy flow in the central rapidity region does not depend on the nature or mass of the colliding projectiles but instead on $\ln \sqrt{s}$. At high energies photons behave like hadron. In this sense, DIS can be looked at as a collision of a photon of $(\text{mass})^2 \approx Q^2$ with protons. The data contained in Fig. 5 have been rebinned in W instead of x and been plotted together with data from hadron colliders in Fig. 6. We obtain a quantitatively striking alignment of the HERA and pp-collider data. Note that the average

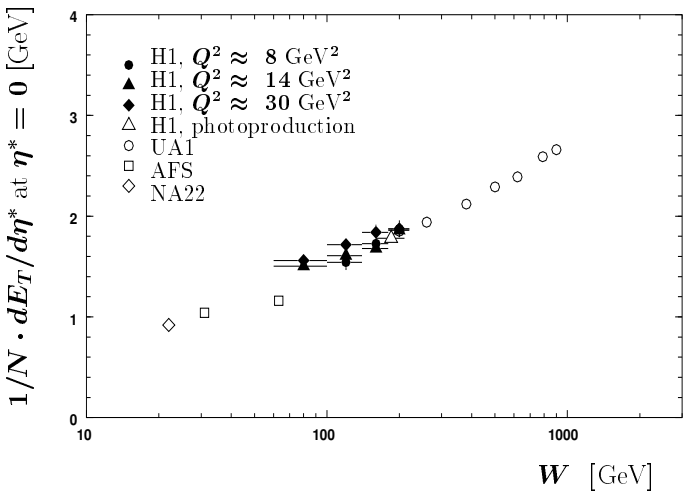

Figure 6: Central transverse energy per unit of rapidity as a function of the center of mass energy in hadronic and e-p collisions.

E_T depends only weakly on Q^2, the (mass)^2 of the virtual photon. The observed dependence on x_{Bj} is translated into the energy dependence on W because of $W^2 \approx y \cdot s = Q^2/x_{Bj}$ at low x_{Bj}. For details of the analysis see [20] and references therein.

The peculiarities of the parton evolution at very low x_{Bj} measured at HERA seem to be relevant to the description of quantities like $< E_T >$ in the rapidity plateau of hadronic collisions! If the validity of the DGLAP and BFKL evolution equation can be distinguished at HERA, new quantitative approaches to the description of hadronic collisions might be envisaged. It would be useful to generate similar plots for other observables like $< p_T >$ or charged and particle multiplicities. However, it might turn out that parton shower and hadronization effects disguise the importance of the evolution equations.

2.2 Forward Jets

The H1 collaboration has analyzed[19] jet production in the forward region to look for additional hints for the BFKL mechanism. According to an idea of Mueller and others [11, 21, 22] the sensitivity to the differences between the two evolution schemes is enhanced, if jets with sufficient $k_T \approx Q$ and $x_{jet} = E_{jet}/E_p \gg x_{Bj}$ are selected. Due to the strong ordering in the DGLAP evolution the phase space under these conditions is strongly suppressed. A measured significant rate of forward jets could be an indicator for the BFKL mechanism.

x range	data events	MEPS events	CDM events	$\sigma(ep \to \text{jet} + X)$ (pb)
$2 \cdot 10^{-4} - 1 \cdot 10^{-3}$	271	141	282	$709 \pm 42 \pm 166$
$1 \cdot 10^{-3} - 2 \cdot 10^{-3}$	158	101	108	$475 \pm 39 \pm 110$

Table 1: Numbers of observed DIS events with a selected forward jet. The measured cross section $ep \to \text{jet} + X$ for forward jets is also given. The errors reflect the statistical and systematic uncertainties.

Jets were selected with a cone algorithm in the space of pseudo-rapidity and azimuthal angle requiring $E_T > 5$ GeV inside the cone. The condition $y > 0.1$ has been imposed to ensure that the current jet is well inside the central region of the detector. For events with $Q^2 \approx 20$ GeV^2

"forward" jets were counted. They are defined by $x_{jet} > 0.025$, $0.5 < k^2_{T,jet}/Q^2 < 4$, $6^0 < \theta_{jet} < 20^0$ and $k_{T,jet} > 5$ GeV, where $k_{T,jet}$ is the transverse momentum of the jet. The resulting number of events observed with at least one forward jet in the kinematic region $160^0 < \theta_e < 173^0$ and $E_e > 12$ GeV is given in table 1 for two bins in the x-interval $2 \cdot 10^{-4} < x < 2 \cdot 10^{-3}$.

The measured rates may be directly compared with the expectations from the Monte Carlo models. Within the application limits of the models, CDM describes the rates better. The cross section is increasing with decreasing x_{Bj}. This might be a further hint that the evolution dynamics obeys only a weak ordering in k_T.

2.3 Discussion

The analysis of jet production and transverse energy flow in the central rapidity region of the γ^*-proton center of mass system opens a new approach to distinguish between the BFKL and DGLAP evolution scheme. As the sensitivity of the F_2 structure functions alone is limited it might be the only way to do this at HERA energies. However, the signatures suffer from large uncertainties of an experimental nature and of a strong model dependence (in particular to the level of hadronization in the Monte Carlos, matching of matrix elements and parton showers in MEPS, account for the proton remnant). A model based on the BFKL evolution including hadronization is urgently needed to proceed further.

3 QCD with Jets

We will now turn to the analysis of the photon fragmentation or current region which is best covered by the HERA detectors. The basic leading order diagrams for two jet production are shown in Fig. 7. The (2+1) jet cross section has two contributions: one is the fusion of a gluon with the virtual photon creating a $q\bar{q}$-pair, known as the boson-gluon fusion (BGF) process, the second is the radiation of a gluon off the struck quark, the so called QCD-Compton graph.

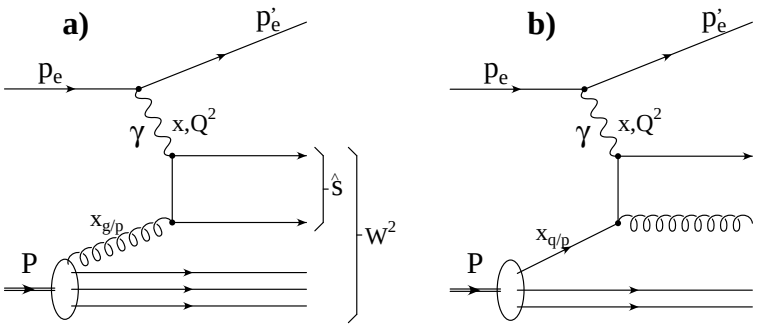

Figure 7: Leading order(α_s) diagrams for 2+1 jet production in DIS for (a) boson-gluon fusion and (b) the QCD-Compton process.

The (2+1) jet cross section can schematically be written as

$$\sigma_{2+1} \sim \alpha_s(Q^2) \cdot \{A \cdot g(x_{g/p}, Q^2) + B \cdot q(x_{q/p}, Q^2)\} \qquad (1)$$

The coefficients A and B can be calculated in perturbative QCD. Note that Bjørken-x is not identical to the fractional momentum $x_{i/p}$ of the parton i initiating the hard sub-process, i standing for either a quark (q) or a gluon (g). $x_{i/p}$ is related to the invariant mass squared of the hard sub-system ($\hat{s}$) in the following way:

$$x_{i/p} = \frac{\hat{s} + Q^2}{ys} = x_{Bj}\left(1 + \frac{\hat{s}}{Q^2}\right) \gg x_{Bj} \tag{2}$$

where $\hat{s}$ can be measured either directly from the invariant mass of all particles belonging to the jets of the hard sub-system or from the jet directions w.r.t. the hadronic center-of-mass system, which is the rest system of the exchanged photon and the proton. Experimentally the parton directions and momenta are approximated by the directions and energies of the jets produced in the fragmentation process.

Depending on the kinematic range in x and Q^2 the (2+1) jet rate can be used to measure the strong coupling constant in a region where the parton distributions g and q are well known. The knowledge of $\alpha_s(Q^2)$ from other experiments can be used to determine the gluon density at low x where the contribution of the boson-gluon fusion diagram dominates. This method is similar to the analysis of multiple jet and direct photon data at proton-colliders, with the advantage that the kinematic variables x and Q^2 can be determined independently by the measured electron. This analysis is more difficult than that of multi jet events at e^+e^--colliders because strongly interacting particles can already be found in the initial state.

3.1 The Determination of $\alpha_s(Q^2)$ from Jet Rates

The running of the strong coupling constant can in principle be determined in a single experiment by varying the Q^2 of the DIS-event. The kinematic region has to be chosen such that parton densities are well known. This implies roughly $x_g > 10^{-2}$ and $x_q \geq 10^{-2}$. Here QCD-Compton and BGF process contribute about the same. Also parton shower effects become sizeable at lower x_{Bj}.

Special care has to be taken to exclude the problematic forward region where besides experimental problems, divergences occur in the calculations of the QCD matrix elements due to collinear partons. H1 chooses an angular cut $10^0 < \theta_{jet} < 145^0$ in the laboratory whereas ZEUS ($0.1 < z < 0.9$) cuts on the variable $z = (p \cdot p_{jet})/(p \cdot q)$, which is related to the angle of the jet w.r.t. the direction of the incoming parton in the γ^*-parton center of mass system. The ZEUS data have an additional cut on the kinematic variable $y > 0.1$.

H1 has already published[23] an early result of the 1993 data based on an integrated luminosity of 0.3 pb^{-1}. A new preliminary results from the 1994 HERA running period is available from ZEUS[24][1] representing 3.2 pb^{-1}. H1 and ZEUS use the modified JADE jet finding algorithm with resolution parameter y_{cut}=0.02. A pseudo particle is introduced to account for the missing longitudinal momentum of the unobserved remnant "(+1)". Pairs of "particles" are combined until all remaining pairs have an invariant mass squared $m_{ij}^2 > y_{cut}W^2$. The jet rates

$$R_{2+1}(Q^2, y_c) = \frac{\sigma_{2+1}(Q^2, y_c)}{\sigma_{1+1}(Q^2, y_c) \; + \; \sigma_{2+1}(Q^2, y_c)} \tag{3}$$

are evaluated in three bins of Q^2 in the range of about 100 to 4000 GeV^2 and as a function of the jet-resolution parameter y_{cut}. The Monte Carlo program MEPS with the MRSH[26] parton

[1] A preliminary new analysis of H1 can be found in [25].

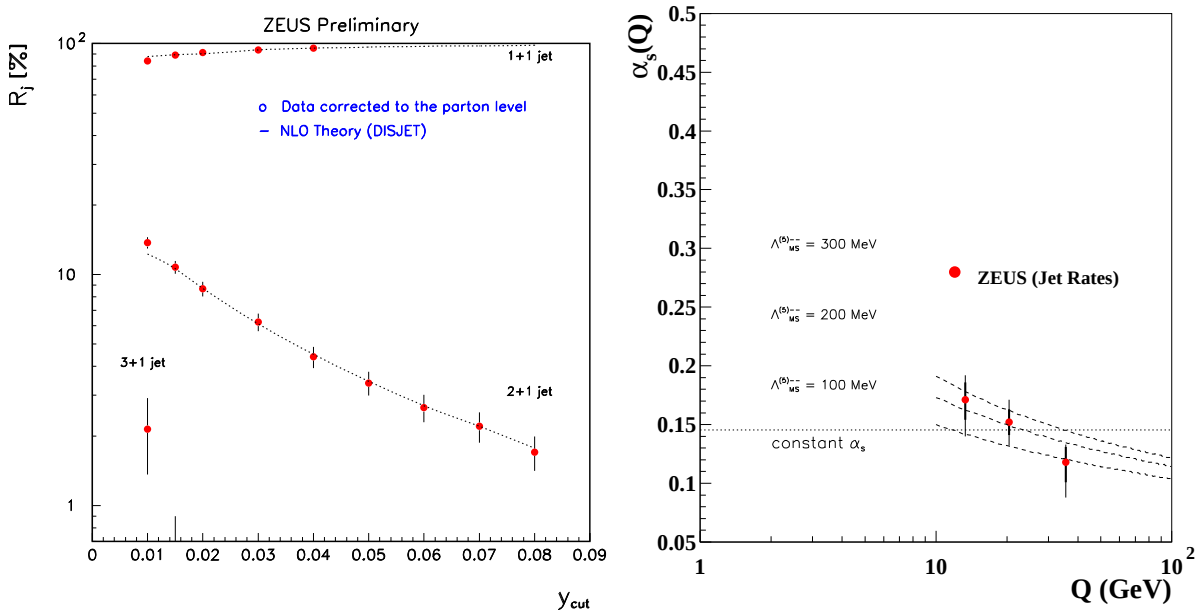

Figure 8: (2+1) Jet rates (ZEUS data) corrected to parton level as a function of the resolution parameter y_{cut} for $240 < Q^2 < 720$ GeV^2. They are compared to the NLO calculation DISJET.

Figure 9: ZEUS data on $\alpha_s(Q)$ from Jet Rates. The solid lines represent α_s with $\Lambda_{5\overline{MS}} = 100, 200$, and 300 MeV. The dashed line is the best fit to a constant α_s hypothesis.

densities is used to correct the jet rates to the parton level. Subsequentially the data are compared to NLO calculations as implemented in the programs PROJET[27] and DISJET[28]. These calculations in next-to-leading order use only the JADE algorithm.

As demonstrated for the ZEUS data in Fig. 8 an excellent description of the data is obtained. The rates $R_{2+1}(Q^2)$ at $y_{cut} = 0.02$ are translated into three measurements of $\alpha_s(Q^2)$. The result of ZEUS is presented in Fig. 9 together with the 2-loop solution of the re-normalization group equation in the $\Lambda_{5\overline{MS}}$ scheme (five flavours) for three different values of $\Lambda_{5\overline{MS}}$. The result of the fit to the combined data within $120 < Q^2 < 3600$ is extrapolated to the Z^0-mass with the result:

$$\alpha_s(M_Z) = 0.117 \pm 0.005(stat)^{+0.008}_{-0.009}(sys) \qquad \text{ZEUS}$$

The published result of H1 is:

$$\alpha_s(M_Z) = 0.123 \pm 0.012(stat) \pm 0.013(sys) \qquad \text{H1}$$

The dominant sources of the systematic error are shared between experimental (hadronic energy scale), hadronization and renormalization and factorization scale uncertainty. The obtained values can be compared to the world average of $\alpha_s(M_Z) = 0.117 \pm 0.005$ [29]. More important is that this unique measurement allows the study of the running of α_s using only one observable at various re-normalization scales in a single experiment.

3.2 Direct Measurement of the Gluon Distribution

At low x the boson gluon fusion process is the dominant source for (2+1) jet production in leading order α_s: if the remaining contribution from QCD-Compton processes can reliably be

subtracted, the (2+1)jet cross section becomes a direct measurement of the gluon density in the proton. In higher orders of α_s, terms containing both, the quark and the gluon density, occur and the contributions cannot easily be separated by a simple subtraction.

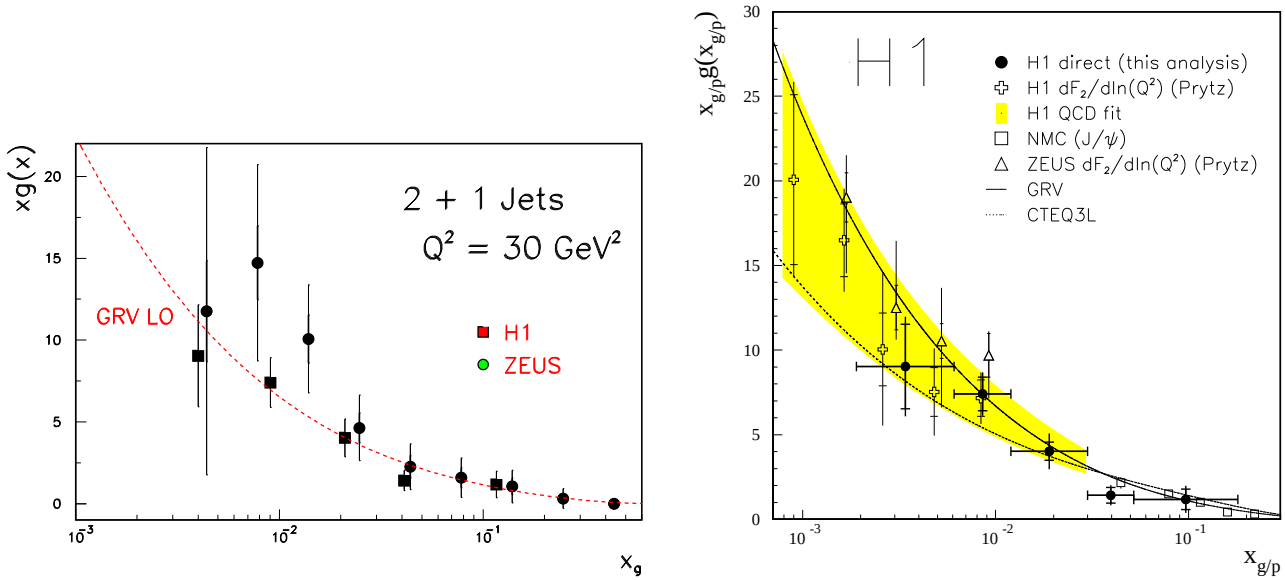

Figure 10: Left: Measured gluon density as function of fractional gluon momentum for H1 (published result of 1993 data) and ZEUS (preliminary 1993 data) at $Q^2 = 30$ GeV^2

Figure 11: Right: The H1 gluon density compared with indirect LO determinations at $Q^2 = 20$ GeV^2 by H1 and ZEUS and with a direct determination from J/ψ production by NMC evolved to $Q^2 = 30$ GeV^2. The lines are two parameterizations of the gluon density, see text.

A cone algorithm in the hadronic center of mass system is used by both collaborations to select the events. The Q^2 range is approximately 10 to 100 GeV^2, corresponding to the low x regime. Again special care has to be taken w.r.t. the forward region: different cuts on the data and at the event generator level are employed by the two collaborations. H1[30] requires $\sqrt{\hat{s}} \geq$ 10 GeV and $10^0 < \theta_{jet} < 150^0$. This required a special adaptation in the LEPTO Monte Carlo code to avoid the regions of divergences. But these cuts use a larger fraction of phase space. For further details see [30]. In the ZEUS analysis the cut is $\hat{s} > y_{min} \cdot W^2$ with $y_{min} = 0.0025$. After these cuts samples of 328 and 935 events with (2+1)jets have been obtained by H1 and ZEUS for the 1993 data, analyzing an integrated luminosity of 0.24 pb^{-1} and 0.52 pb^{-1}, respectively. They are in the fractional momentum range $0.002 \lesssim x_{g/p} \lesssim 0.2$ and in the Bjørken-x range of $0.0003 \lesssim x \lesssim 0.0015$. In this kinematic region and after these cuts the ratio of BGF and QCD-Compton cross sections is approximately 3/1, independent of $x_{i/p}$.

The momentum fraction $x_{g/p} = x_{Bj} \cdot (1 + \hat{s}/Q^2)$ of the parton is calculated from the invariant mass $\sqrt{\hat{s}}$ of the jets on an event by event basis. The Monte Carlo code LEPTO with MEPS (MRSH parameterization[26]) was used to calculate the contribution from BGF and QCD-Compton in LO. These and the correlation between the reconstructed $x_{g/p}^{rec}$ and the generated parton quantities $x_{g/p}$ containing all effects due to parton showers, hadronization and detector performances have been used in an unfolding program [31] to derive the gluon density. The results of the H1 and ZEUS (preliminary) data are presented in Fig. 10. Not included in the errors is a global 11% normalization uncertainty. The systematic errors of the ZEUS analysis are presently larger, mainly due to the large sensitivity to the parameter y_{min}.

In Fig. 11 the H1 result is confronted with other LO determinations of the gluon density: the analysis of the F_2 scaling violations by H1[32] and ZEUS[33] at $Q^2 = 20$ GeV^2 and a determination from J/ψ production by NMC[34] which has been evolved from $Q^2 = 1.5$ GeV^2 to 30 GeV^2. All gluon densities determined in leading order agree very well within their errors.

The results are further compared with two different LO-parameterizations of the gluon density. The GRV[35] model assumes the gluons and sea quarks to be valence-like at $Q^2 = 0.23$ GeV^2 and the growth of the gluon density with decreasing $x_{g/p}$ values is due to radiation of low x partons generated according to the Altarelli-Parisi evolution equations. The CTEQ3L[36] parameterizations are based on input distribution functions at $Q^2 = 4$ GeV^2 assuming the sea and gluon distributions to have the same power dependence of the fractional momentum x_g. Within the present errors both are consistent with the H1 result.

4 Exclusive Final States

In this section I will address results on light and heavy vector meson production, both in photo-production ($Q^2 \approx 0$) and in DIS. Vector meson production has been studied intensively in hadron-hadron and photon-hadron collisions. The elastic production of the light vector mesons has been described successfully by the vector dominance model based on the exchange of a soft pomeron[37, 38]. The elastic cross section is related to the total cross section σ_{tot} by the optical theorem:

$$\left.\frac{d\sigma_{el}}{dt}\right|_{t=0} \sim \sigma^2_{tot}(W_{\gamma p}) \sim W^{4\varepsilon}_{\gamma p} \qquad \text{with} \quad \varepsilon \approx 0.0808 \tag{4}$$

Therefore the elastic production cross section rises in this model only slowly with the center of mass energy $W_{\gamma p}$ of the photon-proton system. The flat behaviour $\sim W^{2\varepsilon}_{\gamma p}$ of the total γp-cross section has been observed up to the highest energies available at HERA, in strong contrast to the virtual $\gamma^* p$-cross section which increases strongly with $W_{\gamma p}$ for all $Q^2 \gtrsim 5$ GeV^2 [5, 39, 40] as a consequence of the rising gluon density at low x. Data from HERA on vector meson production at high Q^2 will be presented.

Boson-gluon fusion is the dominant production mechanism for J/ψ-mesons in hadronic collisions. The measurement of J/ψ production has been suggested as a tool to probe the gluon density of the proton at HERA. The interesting question occurs, if J/ψ elastic photo-production follows the soft VDM behaviour like the light vector mesons. The mass of the J/ψ may introduce a hard scale due to its high mass which might lead to a break-down of the soft VDM.

We address two physics topics in this section: the nature of the Pomeron and the relation to the rise of the gluon density at low x.

4.1 Elastic J/ψ Production at $Q^2 \approx 0$ GeV^2

Three different possible diagrams for J/ψ production in photon proton collisions are introduced in Fig. 12. The first graph represents the discussed VDM process with a pomeron exchange between the proton and the virtual photon after it has fluctuated into a vector meson[41]. This process predicts a slow increase of the cross section with energy. The second graph illustrates a model by Ryskin[42] inspired by perturbative QCD. A gluon ladder is exchanged to generate the J/ψ. In this model the cross section behaves like

$$\sigma_{elastic}(J/\psi) \sim [\alpha_s \cdot x_g \cdot g(x_g, \mu^2)]^2 \qquad x_g \approx M^2_{J/\psi}/W^2 \qquad \mu^2 \approx M^2_{J/\psi}/4 \tag{5}$$

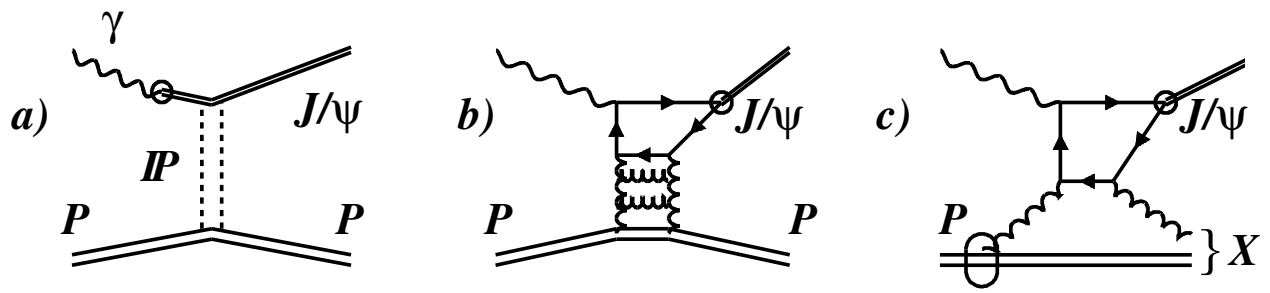

Figure 12: Three different diagrams for J/ψ production in photon proton collisions: a, b for elastic production and c for inelastic production

and is a sensitive probe of the gluon density at x_g.

Elastic events are selected by their clean two track signature. A contribution of order 15-20% from proton-dissociation has to be subtracted. The measured elastic ep cross section is converted into a γp cross section using the Weizsäcker-Williams approximation[43]. The results of both experiments [44, 45] are presented as a function of the photon-proton center-of-mass energy, $W_{\gamma p}$ in fig. 13. For comparison measurements at fixed-target experiments at lower

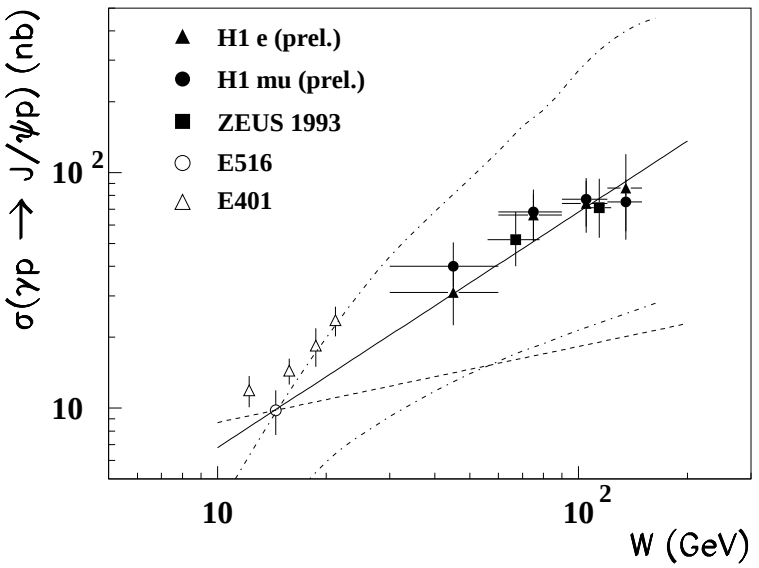

Figure 13: Photo-production cross section for elastic J/ψ production as a function of $W_{\gamma p}$. The filled squares (circles and triangles) represent results of the ZEUS (H1) analyses and the other symbols earlier measurements by fixed-target experiments.

energies and various theoretical predictions are included. A significant rise of the cross section is observed as a function of $W_{\gamma p}$, both with respect to low energy measurements and in the HERA data alone. The rise cannot be accounted for by soft pomeron models [37] however it is in fair agreement with the perturbative QCD model by Ryskin[42]: the dashed (solid) line shows $\sigma_{\gamma p} \sim W_{\gamma p}^{4\varepsilon}$ with $\varepsilon = 0.081$ ($\varepsilon = 0.25$). Both curves are normalized to the E516 data point. The band spanned by the dashed-dotted lines indicates the prediction of the Ryskin model, using the upper and lower limits of the gluon density derived in LO from F_2[33].

Eventually this measurement should allow an extraction of the gluon density, once experimental and theoretical uncertainties are under better control.

4.2 Inelastic J/ψ Production at $Q^2 \approx 0$ GeV^2

Fig. 12c describes the case of inelastic J/ψ production in photo-production. The boson-gluon fusion graph and the subsequent emission of a gluon to produce a colour singlet final state can be calculated in the framework of the colour singlet model[46] in next-to-leading order. Because the emitted gluon is not confined to the proton, the process is less constrained and the resulting energy dependence on the gluon density is weaker than in the case of Fig. 12b.

$$\sigma_{inelastic}(J/\psi) \sim \alpha_s^2 \cdot [x_g \cdot g(x_g, \mu^2)] \qquad x_g \approx 1/W^2 \cdot \{M_{J/\psi}^2/z \ + ... + ...\} \tag{6}$$

where $z = \frac{p \cdot p_\psi}{p \cdot q} = [E_{J/\psi}/E_\gamma]$ is the inelasticity parameter, (z=1.0 defines elastic events).

Muon and electron pairs have been selected for $z < 0.9$ and the photo-production cross section has been derived from this measurements. The result of the 1994 and 1993 data by H1[45] and ZEUS[47] respectively, is shown in fig. 14 as a function of $W_{\gamma p}$ and compared to

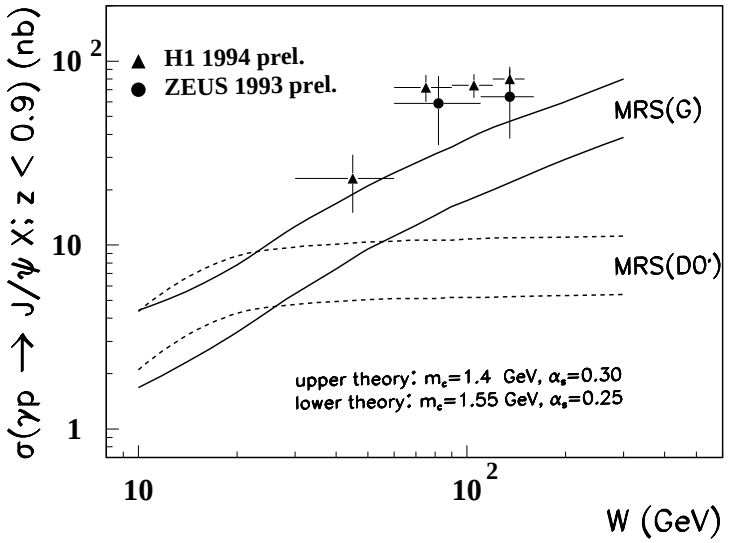

Figure 14: Photo-production cross section for inelastic J/ψ production as a function of $W_{\gamma p}$. The theoretical curves are NLO calculations for different proton parton density parameterizations. The upper and lower curves indicate the uncertainty due to variations of the mass of the charm quark and the strong coupling constant.

NLO calculation [46] for two different parameterizations of the parton densities in the proton and for two different values of the charm quark mass and the strong coupling constant, which are the main sources of theoretical uncertainty. The measured cross section is almost a factor two above the the highest prediction.

The $W_{\gamma p}$ dependence is best described, if a gluon density distribution function is used which increases towards low x, such as MRS G [50]. The deviation in the normalization is smallest, if $\alpha_s \approx 0.3$ (a rather large value), and $m_c \approx 1.4$ GeV^2 (a comparatively low value). This difference in absolute magnitude of the cross sections is under investigation[2].

[2]New calculations are becoming available now which give a better description of the data[48, 49].

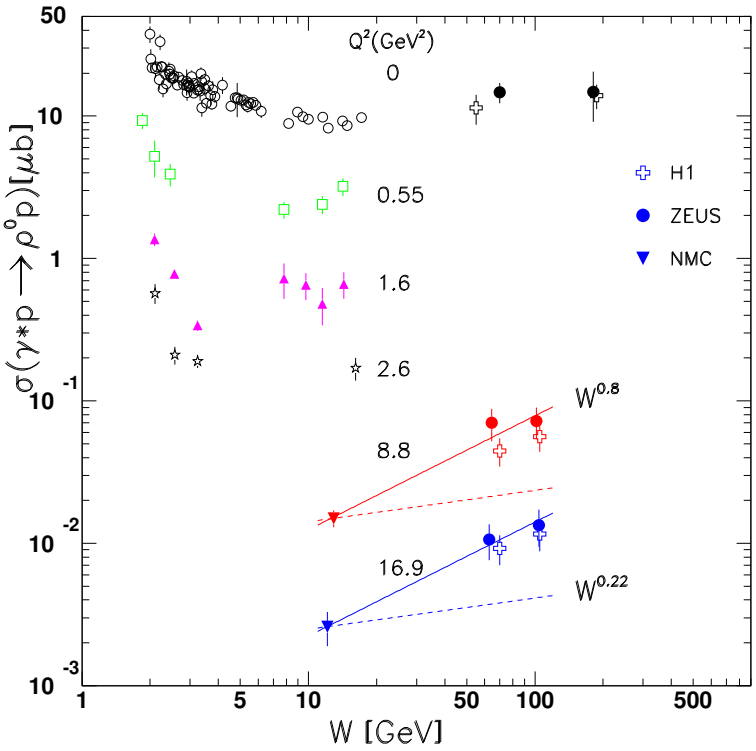

Figure 15: ρ^0 production at high Q^2 as function of $W_{\gamma^* p}$. The H1 data are preliminary! The low energy data ($W < 20$ GeV) come from fixed target experiments.

4.3 ρ^0 Meson Production at Low and High Q^2

The exclusive production of the light vector mesons is of particular interest(we discuss only the ρ^0 in the following although data on the ϕ have become available recently). Due to their small mass we are able to vary the scale in the scattering process by changing Q^2 from 0 GeV^2 in photo-production to high values of Q^2 in DIS. While numerous data exist for low Q^2, only two experiments have published results in DIS for $Q^2 > 5$ GeV^2, the EMC[51] and NMC[52] collaborations, but at relative small $W < 20$ GeV. The low Q^2 and photo-production data are well described by the VDM not only in the slow growth of the cross section with the center of mass energy, but also in its Q^2 dependence which follows approximately $1/Q^4$[37].

At HERA data have been collected at larger Q^2 and high W up to 100 GeV. Treating the pomeron as an exchange of two gluons in perturbative QCD similar to [42] for the J/ψ, calculations are now available also for light vector mesons[53, 54]. Brodsky et al.[55] have studied this process in double leading logarithm approximation (DLLA). They predict that at high Q^2 the vector mesons should be produced dominantly by longitudinal polarized photons. The cross section should have a steep slope in Q^2 and be proportional to the square of the gluon density in the proton, similar to equation(5):

$$\left.\frac{d\sigma^L_{elastic}(\rho^0)}{dt}\right|_{t=0} \sim \alpha_s^2(Q^2)/Q^6 \cdot \left|\left[1 + i(\pi/2)\left(\frac{d}{d\ln x}\right)\right] x_g \cdot g(x_g, Q^2)\right|^2 \quad \text{with} \quad x_g \approx Q^2/W^2 \quad (7)$$

The present HERA data of H1 and ZEUS are not yet accurate enough to test the Q^2 dependence. For details see [56]. We will therefore turn to the measurement of the cross section $\gamma^* p \to \rho^0 p$

as a function of W in intervals of Q^2.

The virtual photon-proton cross section derived from the measured differential electroproduction cross section is shown in Fig. 15 as a function of W and for different average Q^2-values. The HERA data at $Q^2 = 8.8$ and 16.9 GeV^2 are based on 2.9 pb^{-1} in 1994 and 0.55 pb^{-1} in 1993 for the H1[57] and ZEUS[56] experiment, respectively. They exhibit a considerably higher cross section than the NMC points of the same Q^2. This indicates a much steeper slope than the elastic photo-production cross section which follows a $\sim W^{0.22}$ behaviour. This is close to the proportionality of equation (4) which would come out as $W^{0.32}$. The high Q^2-data follow approximately a line described by $W^{0.8}$.

A quantitative comparison has been undertaken by the ZEUS collaboration using equation(7) to calculate the cross section $\sigma(\gamma^* p \rightarrow \rho^0 p)$ as a function of x and for two values of Q^2. The ratio σ^L/σ^T can experimentally be deduced from the ρ^0 density matrix element r_{00}^{04} which can be measured by the decay angular distribution. The result for this calculation shows agreement between data and theory within a wide band of uncertainty. For details consult [56]. More data may turn this type of analysis into a further tool to measure directly the gluon distribution.

5 Summary

Hadronic final states in a new domain of energy have been studied in electron proton scattering at HERA. In this paper I have discussed the following topics:

From the measurement of multi-jet events two results were presented.

- The strong coupling constant α_s was determined in NLO as a function of Q in a single experiment. The extrapolation to the Z^0-mass gives $\alpha_s(M_Z) = 0.117 \pm 0.005^{+0.008}_{-0.009}$ and $\alpha_s(M_Z) = 0.123 \pm 0.012 \pm 0.013$ for the two experiments ZEUS and H1, respectively. These values are in agreement with the combined world data and will become competitive with more data.
- A direct determination of the rising gluon density in LO down to $x_g \approx 2 \cdot 10^{-3}$ confirms the LO derivation from the F_2 structure function.

An analysis of the E_T flow and jet production in the forward region has been attempted to distinguish between the DGLAP and BFKL parton evolution dynamics.

- At low x_{Bj} the transverse energy $dE_T/d\eta^*|_{\eta^*=0}$ is at a level of about 2 GeV and increasing modestly with decreasing x_{Bj}. Within large uncertainties due to hadronization this is consistent with the expectation from BFKL dynamics.
- The central transverse energy $dE_T/d\eta^*|_{\eta^*=0}$ in DIS events at HERA follows the same quantitative energy dependence on $\sqrt{s} = W_{\gamma^* p}$ as proton proton collisions.
- The cross section of forward jet production is rising with decreasing x_{Bj} and is consistent with calculations based on the BFKL dynamics.
- These findings support the BFKL evolution equation, but are not sufficient as a proof.

Exclusive final states are a particular probe for the nature of the pomeron and the gluon density in the proton.

- The elastic production cross section of vector mesons obeys an approximately linear dependence on the center-of-mass energy when a "hard" scale is involved in the process. This scale is reached either at high Q^2 or when the mass of the vector meson is large, as in the case of the J/ψ. The data cannot be described in terms of a soft pomeron exchange but are compatible with models of a hard pomeron based on a gluon ladder exchange.

The study of the hadronic final states in DIS offers new ways to probe the gluon density directly and to study the nature of the pomeron.

Acknowledgments

It is a pleasure to thank everybody of the ZEUS and H1 collaborations who provided such interesting results and who spend much time with me discussing the physics in course of the preparations for this talk. Special thanks go to A. Caldwell, A. DeRoeck, R. Eichler, G. Grindhammer, J. Hartmann, M. Kuhlen and H. Steiner for reading the manuscript and their constructive comments. I would like to thank Prof. Krzysztof Rybicki and his colleagues for smoothly organizing an enjoyable conference at a splendid place like Cracow.

References

[1] I. Abt et al. (H1 Coll.), "The H1 Detector at HERA," DESY 93-103 (1993).
[2] M. Derrick et al. (ZEUS Coll.), "The ZEUS Detector", Status Report, DESY (1993).
[3] ZEUS Collab., M. Derrick et al., Z. Phys. C65 (1995) 379.
[4] H1 Collab., T. Ahmed et al., Nucl. Phys. B439 (1995) 471.
[5] J. Ciborowski, Review on structure functions, contribution to these proceedings.
[6] H1 Collab., Nucl. Phys. B445(1995)3.
ZEUS Collab., M.Derrick et al., Z. Physik (1995) 93-107.
N. Pavel, "Incl. hadron Distributions in DIS at HERA...," DESY 95-147.
[7] A. Brandt, "Diffractive Processes and Rapidity Gaps", contribution to these proceedings.
[8] Yu. L. Dokshitzer, Sov. Phys. JETP 46 (1977) 641;
V.N. Gribov and L.N. Lipatov, Sov. J. Nucl. Phys. 15 (1972) 438 and 675;
G. Altarelli and G. Parisi, Nucl. Phys. 126 (1977) 297.
[9] E.A. Kuraev, L.N. Lipatov and V.S. Fadin, Sov. Phys. JETP 45 (1972) 199;
Y.Y. Balitsky and L.N. Lipatov, Sov. J. Nucl. Phys. 28 (1978) 282.
[10] A.H. Mueller, Columbia preprint CU-TP-658 (1994).
[11] J. Kwieciński, A.D. Martin, P.J. Sutton, Phys. Rev. D46 (1992) 921.
[12] J. Kwieciński, A.D. Martin, P.J. Sutton and K.Golec-Biernat, Phys. Rev. D50 (1994) 217.
[13] K.Golec-Biernat, J. Kwieciński, A.D. Martin and P.J. Sutton, Phys. Lett. B335 (1994) 220.
[14] G. Ingelman, Proc. of the Workshop on Physics at HERA, Hamburg 1991, eds. W. Buchmüller and G. Ingelman, vol. 3, p. 1366.
[15] L. Lönnblad, Computer Phys. Comm. 71 (1992) 15.
[16] G. Gustafson, Ulf Petterson, Nucl. Phys. B306 (1988);
G. Gustafson, Phys. Lett. B175 (1986) 453;
B. Andersson, G. Gustafson, L. Lönnblad, Ulf Petterson, Z. Phys. C43 (1989) 625.
[17] L. Lönnblad, Z. Phys. C65 (1995) 285;
A. H. Mueller, Nucl. Phys. B415 (1994) 373;
L. Lönnblad, CERN-TH/95-95.
[18] ZEUS Collab., M. Derrick et al., Int. Europhys. Conf. on HEP, paper EPS 0391 (1995).
[19] H1 Collab., Phys. Let. B356 (1995) 118.
H1 Collaboration, I. Abt et al., Z. Phys. C 63 (1994) 377.
[20] H1 Collab., DESY-95-156 / accepted by Phys. Lett. B.
[21] A.H. Mueller, Nucl. Phys. B (Proc. Suppl.) 18C (1990) 125; J. Phys. G17 (1991) 1443.
[22] J. Bartels, A. De Roeck, M. Loewe, Z. Phys. C54 (1992) 635;
W.K. Tang, Phys. Lett. B278 (1992) 363.

[23] H1 Collaboration, T. Ahmed et al., Phys. Lett. B346 (1995) 415.
[24] ZEUS Collab., Int. Europhys. Conf. on HEP, paper EPS 0396 (1995).
[25] H1 Collab., Int. Europhys. Conf. on HEP, paper EPS 0486 (1995).
[26] A.D. Martin, W.J. Stirling and R.G. Roberts, Proc. of the Workshop on Quantum Field Theory and Theoretical Aspects of HEP, eds. B. Geyer and E.M. Ilgenfritz (1993) p. 11.
[27] D. Graudenz, PROJET 4.1, CERN-TH 7420/94.
[28] T. Brodkorb and E. Mirkes, DISJET program manual, MAD/PH/821, 1994.
[29] Particle Data Group, L. Montanet et al., Phys. Rev. D50 (1994) 1173.
[30] H1 Collaboration, I. Abt et al., Nucl. Phys. B449 (1995) 3.
[31] V. Blobel, DESY preprint 84-118, and Proceedings of the 1984 CERN School of Computing Aiguablava (Spain), CERN 1985.
[32] H1 Collaboration, I. Abt et al., Phys. Let. B354 (1995) 494.
[33] ZEUS Collaboration, Phys. Lett. B 345 (1995) 576-588.
[34] New Muon Collaboration, D. Allasia et al., Phys. Lett. B258 (1991) 493.
[35] M. Glück, E. Reya, A. Vogt, Phys. Rev. D46 (1992) 1973;
M. Glück et al., DO-TH-94-24.
[36] H.L. Lai et al., MSU-HEP-41024.
[37] A. Donnachie and P.V. Landshoff, Nucl. Phys. B244 (1984), 322; Nucl. Phys. B311 (1989), 509; Phys. Lett. B348 (1995), 213.
[38] A. Donnachie and P.V. Landshoff, Phys. Lett. B185 (1987), 403.
[39] A. Levi, DESY 1995-003.
[40] B. Foster, DESY 1995-158.
[41] J.J. Sakurai, Phys. Rev. Lett. 22 (1969), 981.
[42] M. Ryskin, Z. Phys. C57 (1993), 89.
[43] C.F. Weizsäcker, Z. Phys. 88 (1934), 612
E.J. Williams, Phys. Rev. 45 (1934), 729.
[44] M. Derrick et al. (ZEUS Coll.), Phys. Lett. B350 (1995), 120.
Int. Europhys. Conf. on HEP, paper EPS 0386 (1995).
[45] H1 Collab., Int. Europhys. Conf. on HEP, paper EPS 0468 (1995).
[46] M. Kraemer, J. Zunft, J. Steegborn, and P.M. Zerwas, Phys. Lett. B348 (1995), 657.
[47] ZEUS Collab., Int. Europhys. Conf. on HEP, paper EPS 0387 (1995).
[48] M. Kraemer, DESY 95-46.
[49] M. Kraemer, DESY 95-155.
[50] A.D. Martin, R.G. Roberts, and W.J. Stirling, RAL-94-055 (1994)
[51] EMC Collab., J.J.Aubert et al., Phys. Lett. 161B (1985) 203;
J. Ashman et al., Z. Phys. C39 (1988) 169.
[52] NMC Collab., P. Amaudruz et al., Z. Phys. C54 (1992) 239;
M. Arneodo et el., Nucl. Phys. B429 (1994) 503.
[53] J. Nemchik et al., Phys. Lett. B341 (1994) 228.
[54] I.F. Ginzburg et al., subm. to Nucl. Phys. B (1994).
[55] S.J. Brodsky et al., Phys. Rev. D50 (1994) 3134.
[56] M. Derrick et al. (ZEUS Coll.), DESY 95-133 (1995) accepted by Phys. Lett. B
[57] H1 Collab., Exclusive ρ^0 production in DIS at HERA, Int. Europhys. Conf. on HEP, paper EPS 0490 (1995).